Supplementary Materials

Rational design of fullerene derivatives for improved stability of p-i-n perovskite solar cells

Victoria V. Ozerova [1], Alexander V. Mumyatov [1], Andrey Goryachev [2], Ekaterina A. Khakina [3,4], Alexander S. Peregudov [3], Sergey M. Aldoshin [1] and Pavel Troshin [1,*]

[1] Federal Research Center for Problems of Chemical Physics and Medicinal Chemistry, Russian Academy of Sciences, Academician Semenov Avenue 1, 142432 Chernogolovka, Moscow Region, Russia

[2] Ariel University, Physics Department, Ramat HaGolan St. 65, Ari'el, 40700, Israel

[3] A. N. Nesmeyanov Institute of Organoelement Compounds of Russian Academy of Sciences, Vavylova st. 28, Moscow, 119334, Russia

[4] National Research University Higher School of Economics, Vavylova st. 7, Moscow, 101000, Russia

* Correspondence: troshin2003@inbox.ru

Contents

Figure S17. ^{1}H (a) and ^{13}C (b) NMR spectra of the fullerene derivative **F8**. Assignment of some signals is shown on the insets.

Figure S18. ^{1}H-^{1}H COSY (a) and ^{1}H-^{13}C HMQC (b) NMR spectra of the fullerene derivative **F8** ($CDCl_3$).

Figure S19. PL spectra of the lead halide perovskite films before (black line) and after (red line) deposition of fullerene-based ETLs.

Figure S20. Overview of perovskite/ETL bilayer stack morphology: topography (left column) and IR s-SNOM images recorded at the characteristic frequencies of the ETL material (middle column) and perovskite absorber (right column). The used fullerene derivatives are listed on the left side.

Figure S21. Dependence of the perovskite solar cell parameters on the deposition rate of the fullerene derivative **F1** (20.2 mg mL^{-1} solution in chlorobenzene) used to form electron transport layer in the devices

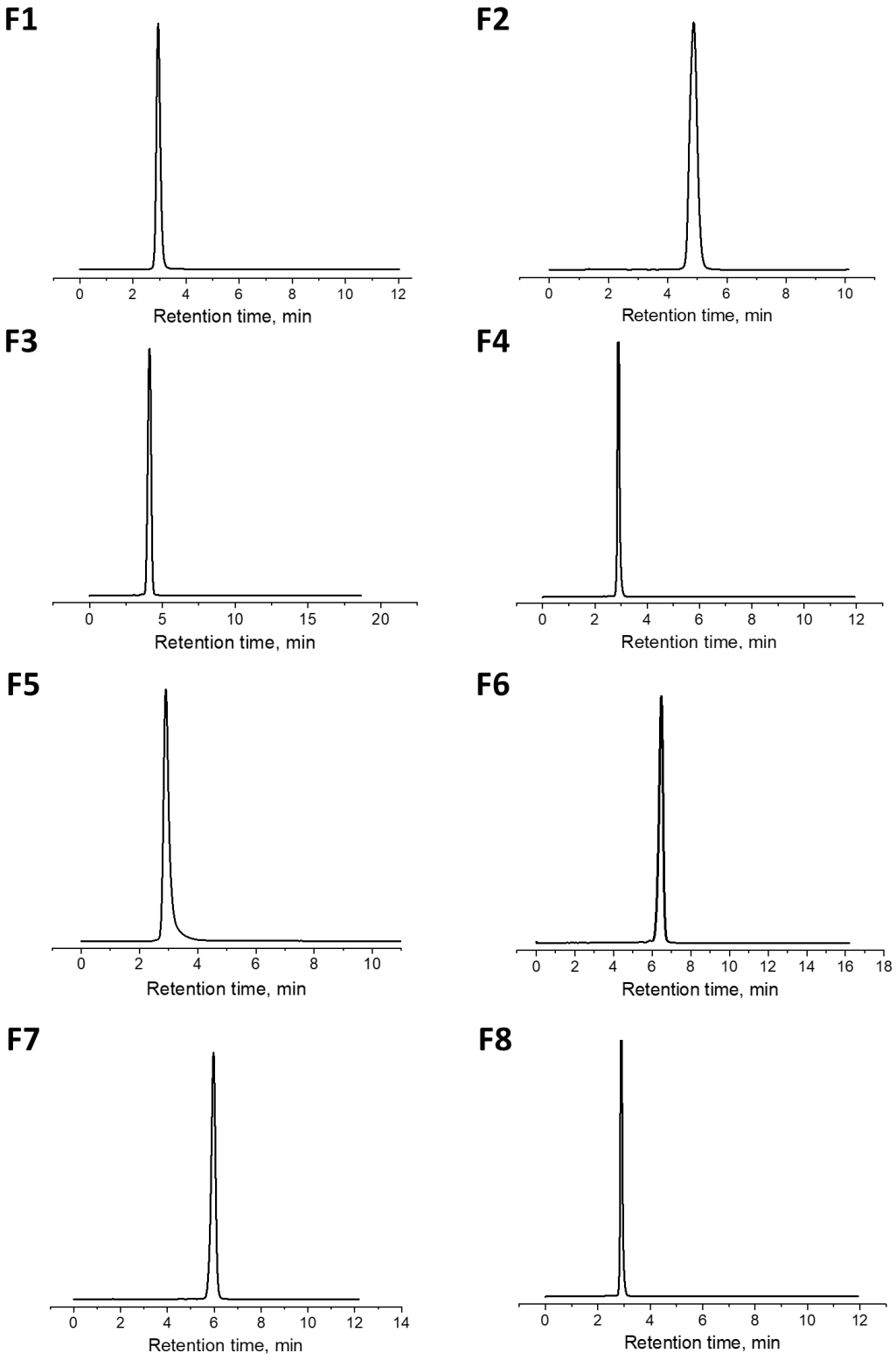

Figure S1. HPLC traces of purified fullerene derivatives **F1-F8**. Phenomenex Luna 5u C18 (2) 100A, 4,6x150 mm analytical column, toluene (40%) – acetonitrile (60%) mixture used as eluent, flow rate 1 mL min^{-1}

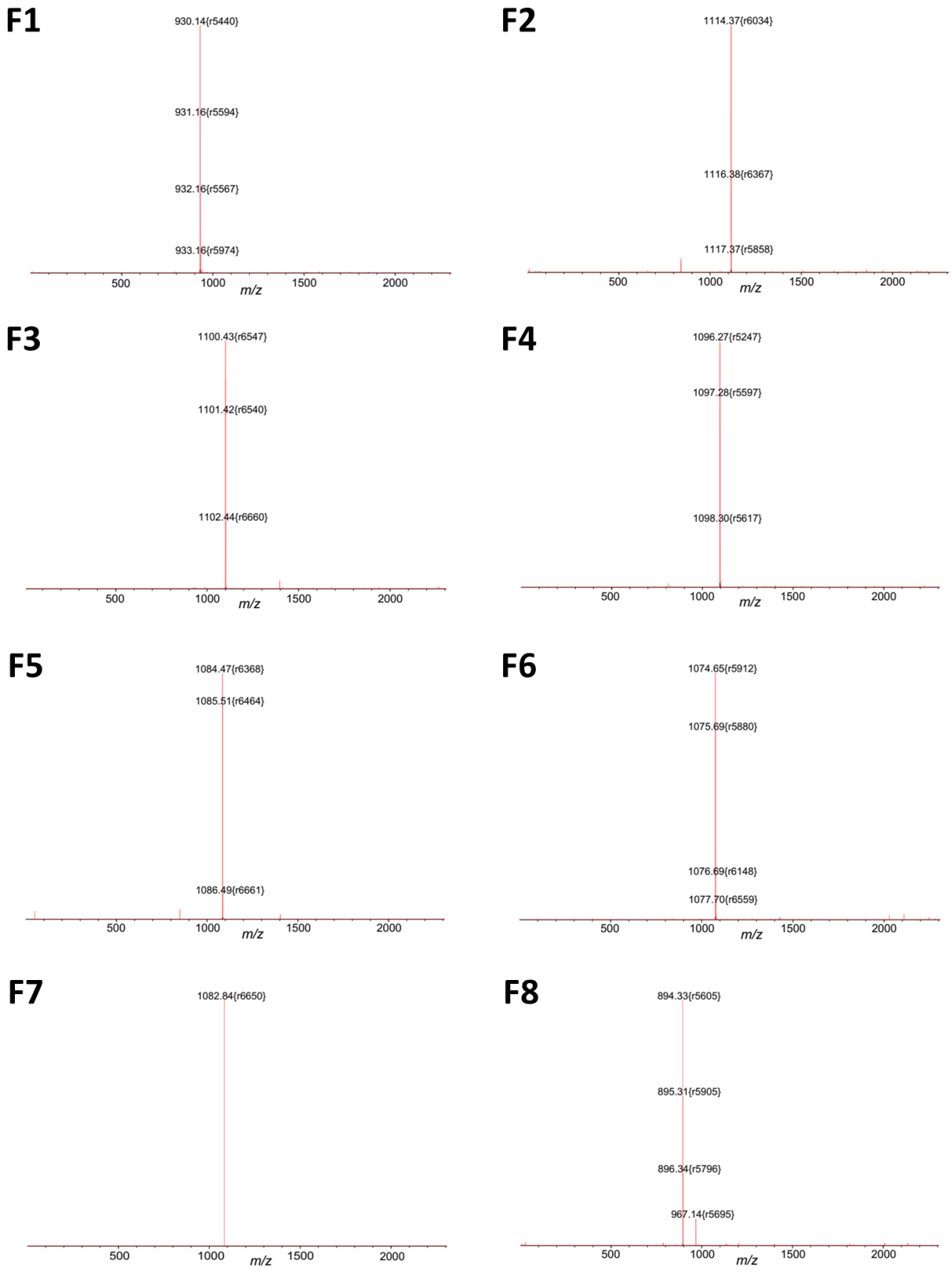

Figure S2. MALDI ToF mass spectra of purified fullerene derivatives **F1-F8**.

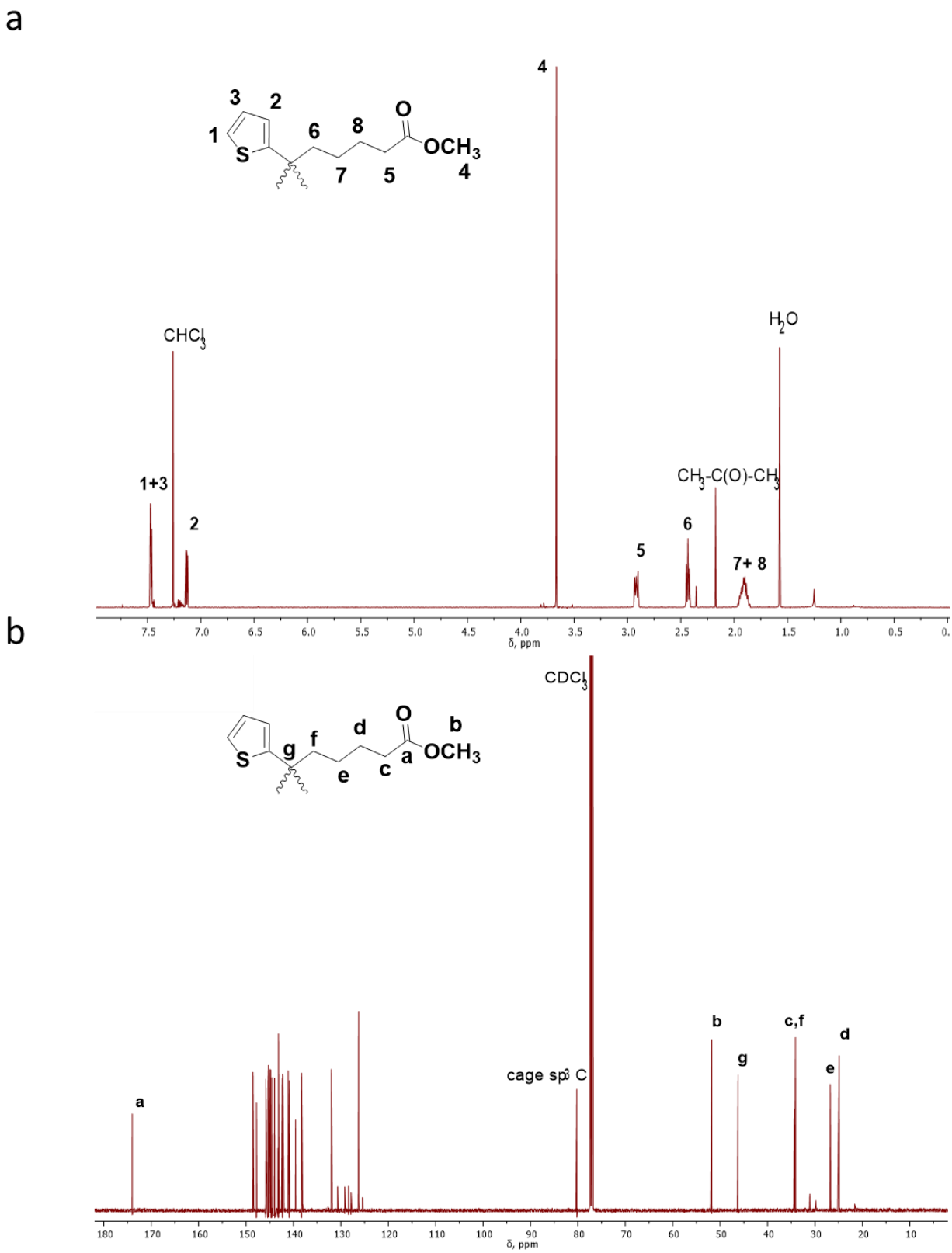

Figure S3. ^{1}H (a) and ^{13}C (b) NMR spectra of the fullerene derivative **F1**. Assignment of some signals is shown on the insets.

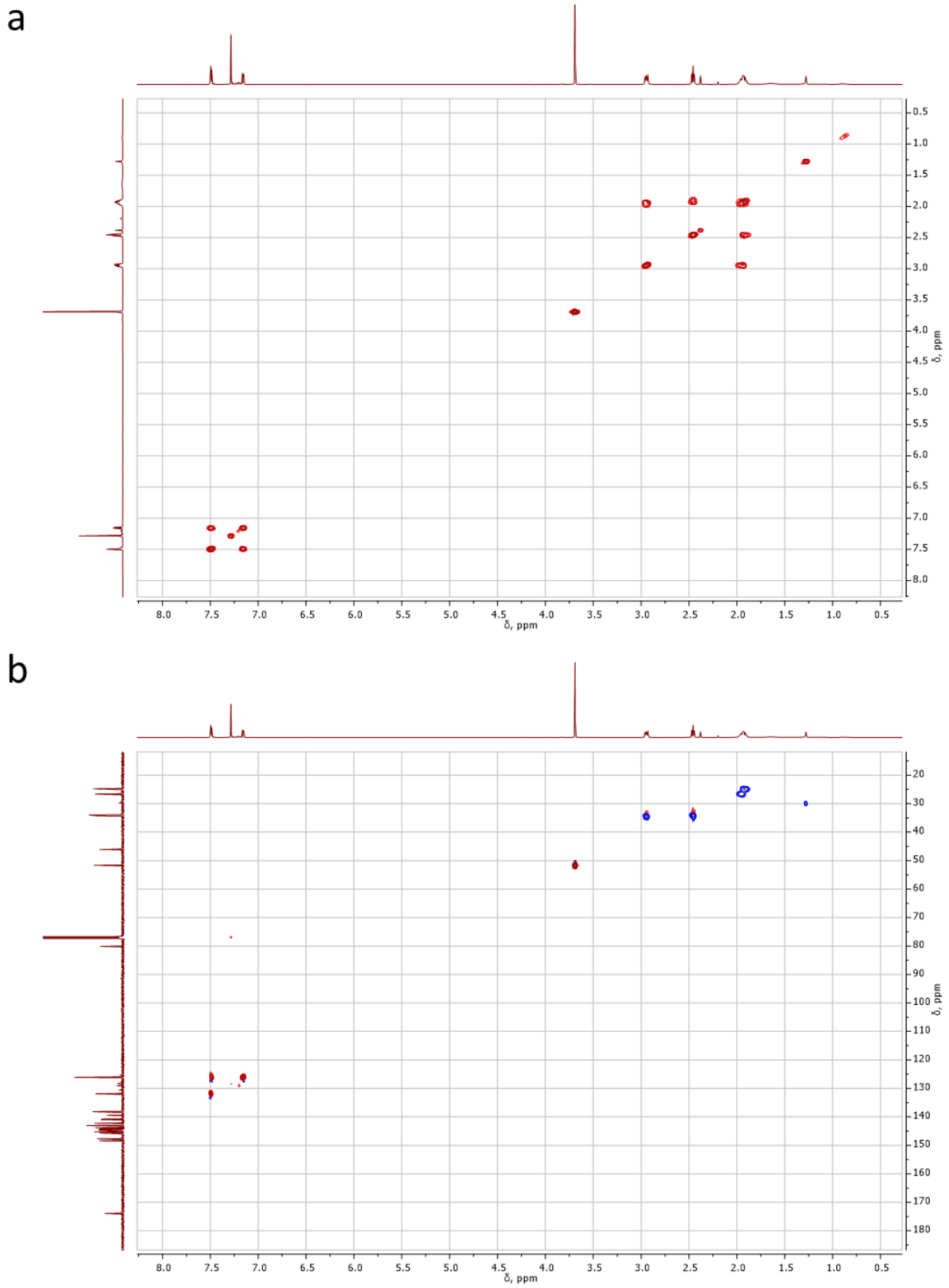

Figure S4. ^{1}H-^{1}H COSY (a) and ^{1}H-^{13}C HSQC (b) NMR spectra of the fullerene derivative **F1** ($CDCl_3$).

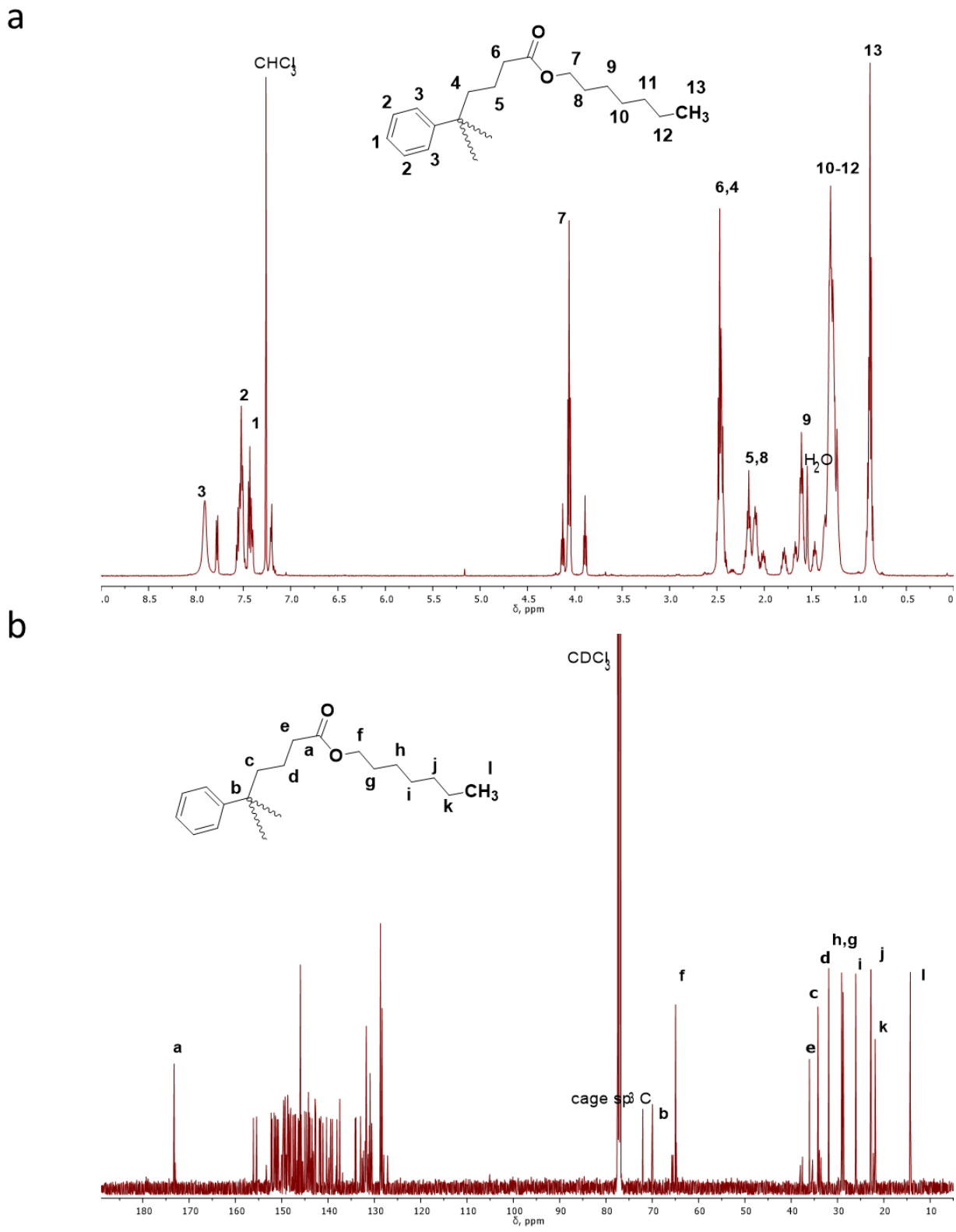

Figure S5. ^{1}H (a) and ^{13}C (b) NMR spectra of the fullerene derivative **F2**. Assignment of some signals is shown on the insets.

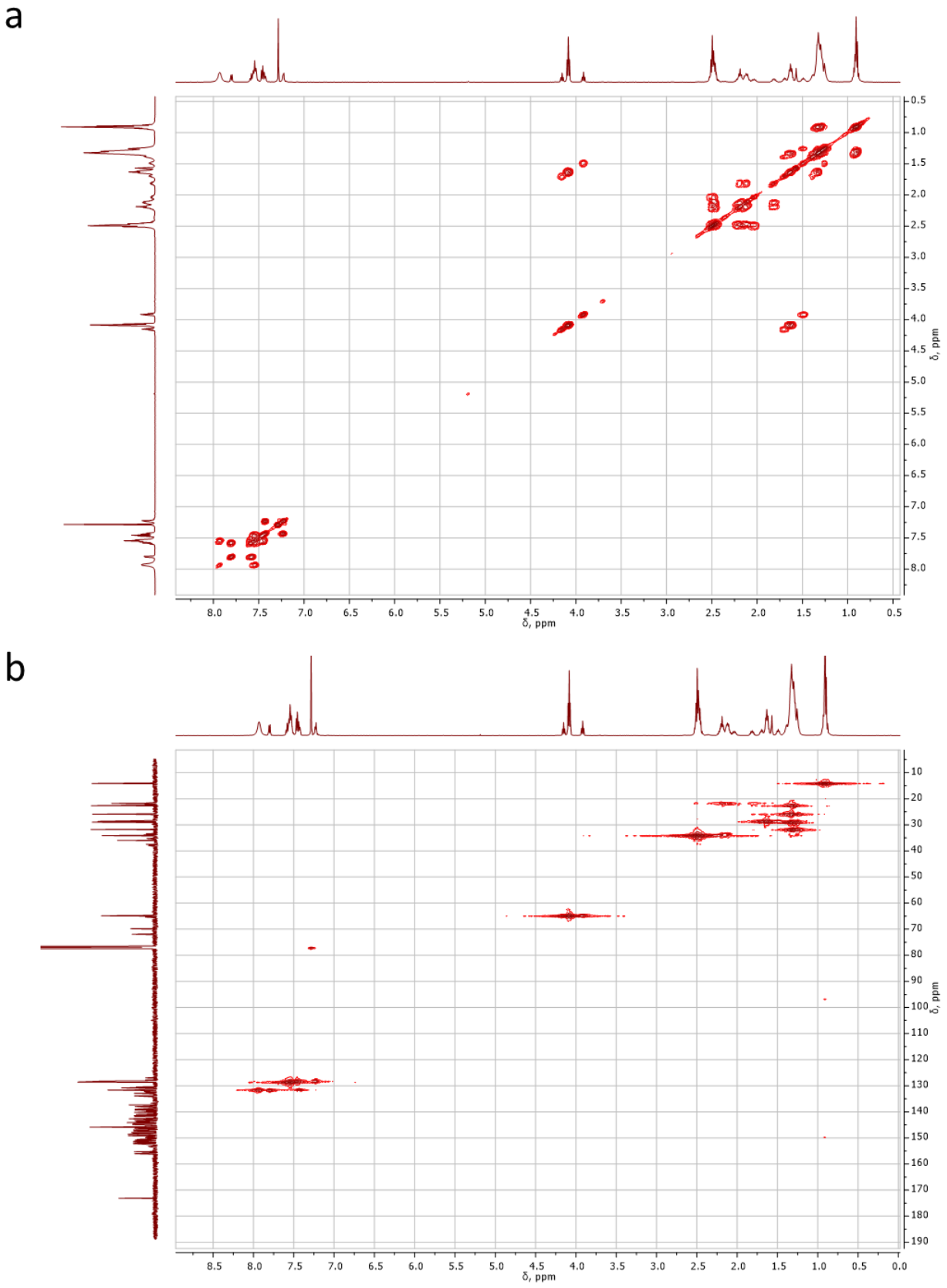

Figure S6. ^{1}H-^{1}H COSY (a) and ^{1}H-^{13}C HMQC (b) NMR spectra of the fullerene derivative **F2** ($CDCl_3$).

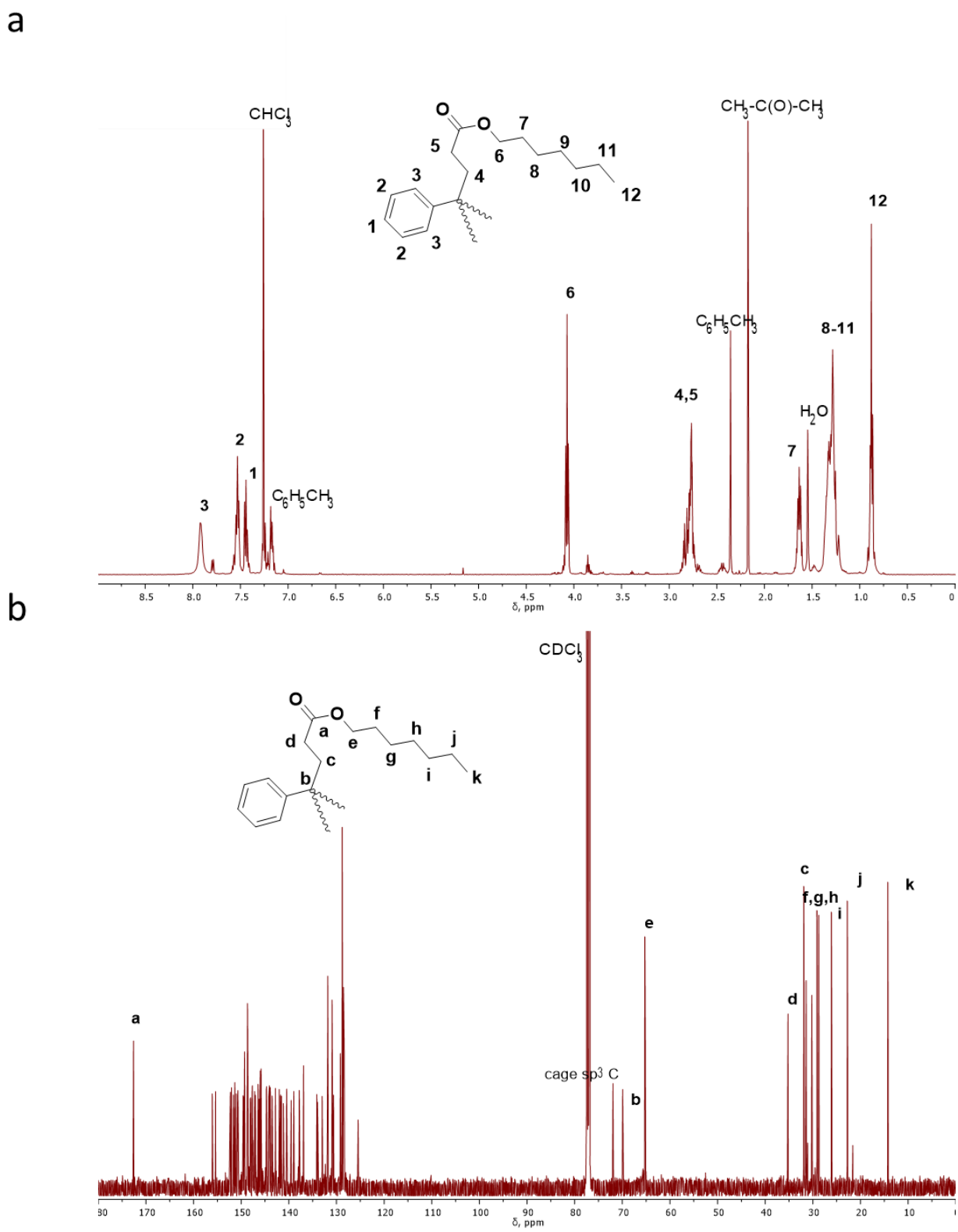

Figure S7. ^{1}H (a) and ^{13}C (b) NMR spectra of the fullerene derivative **F3**. Assignment of some signals is shown on the insets.

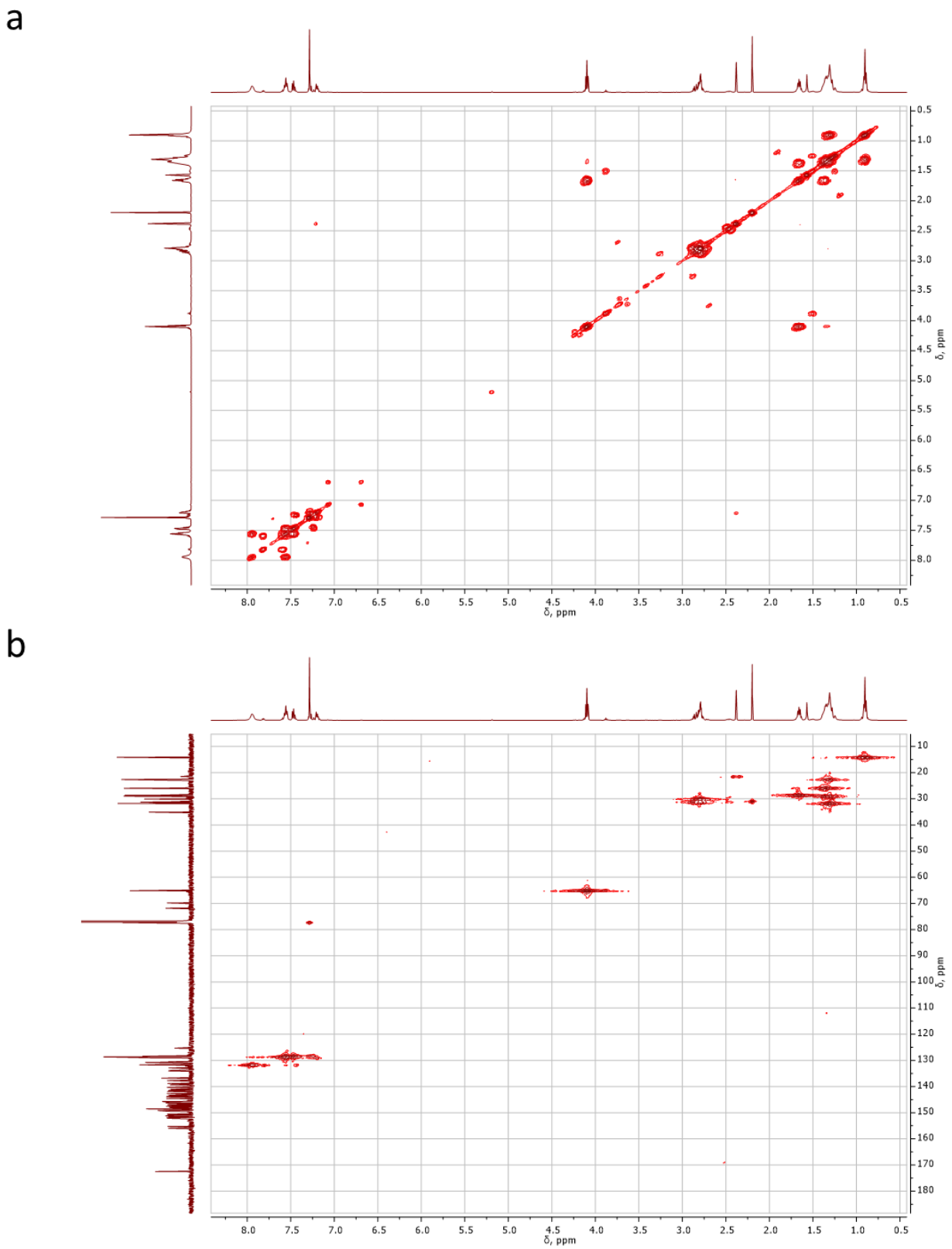

Figure S8. ^{1}H-^{1}H COSY (a) and ^{1}H-^{13}C HMQC (b) NMR spectra of the fullerene derivative **F3** ($CDCl_3$).

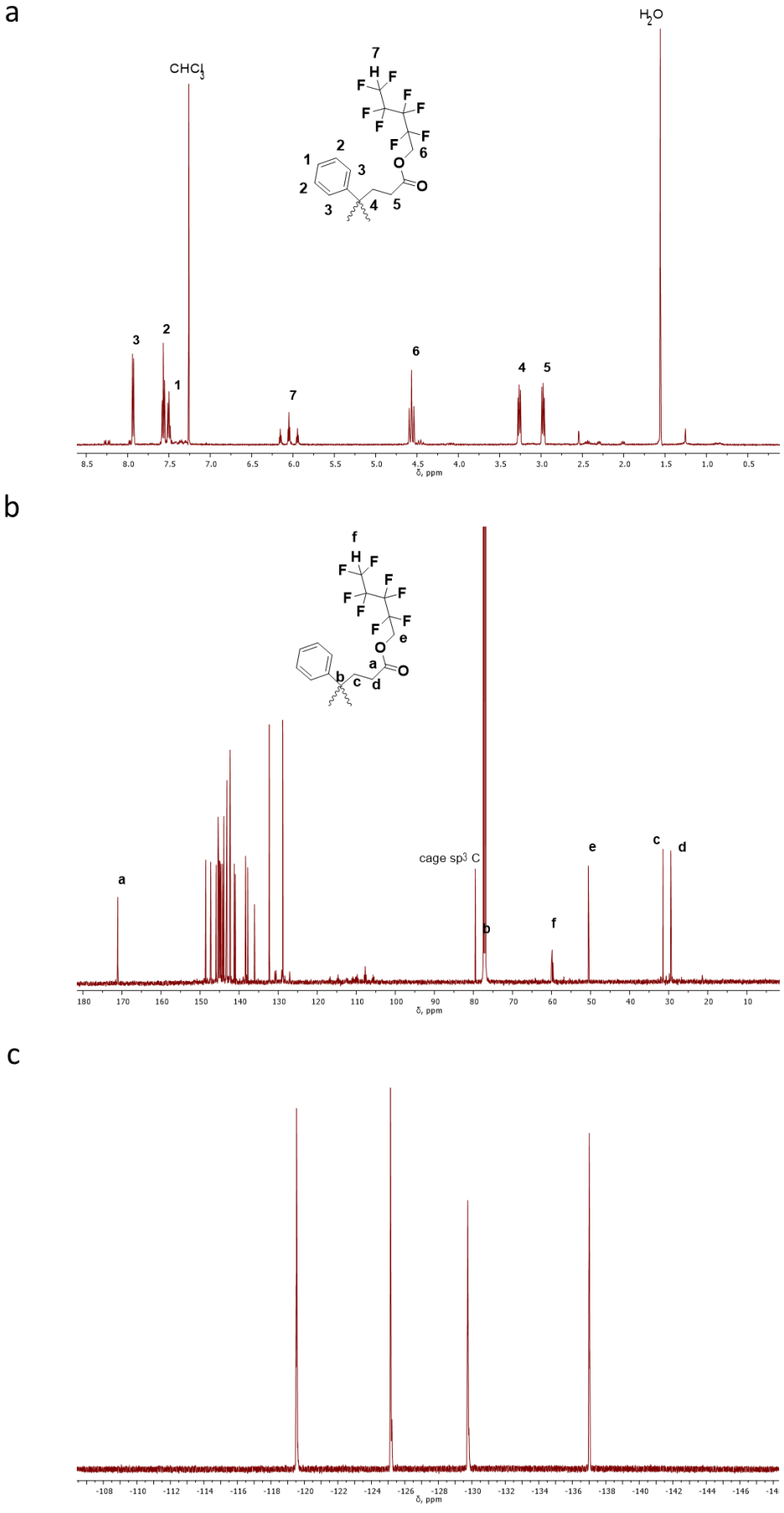

Figure S9. ^{1}H (a), ^{13}C (b) and ^{19}F (c) NMR spectra of the fullerene derivative **F4**. Assignment of some signals is shown on the insets.

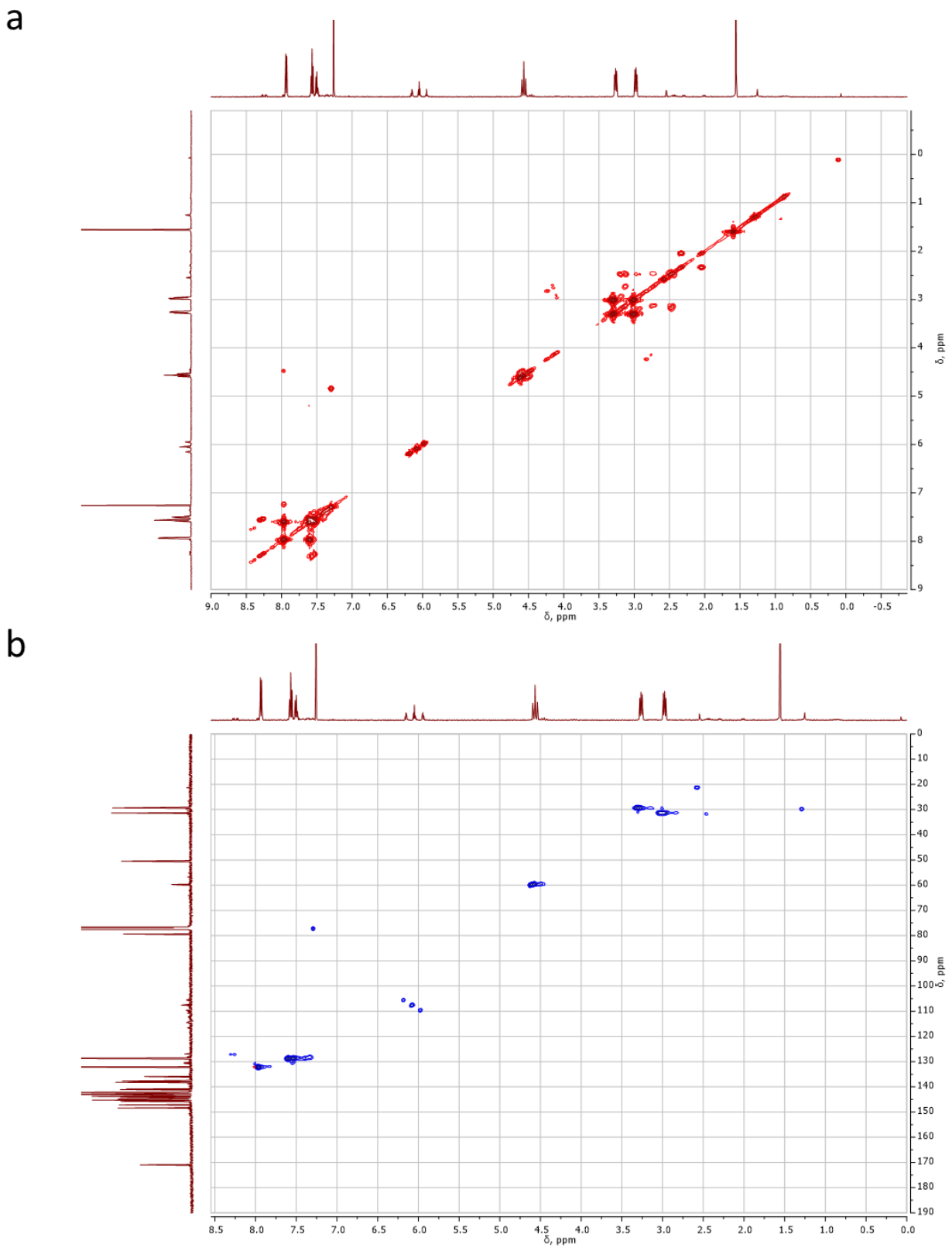

Figure S10. ^{1}H-^{1}H COSY (a) and ^{1}H-^{13}C HMQC (b) NMR spectra of the fullerene derivative **F4** ($CDCl_3$).

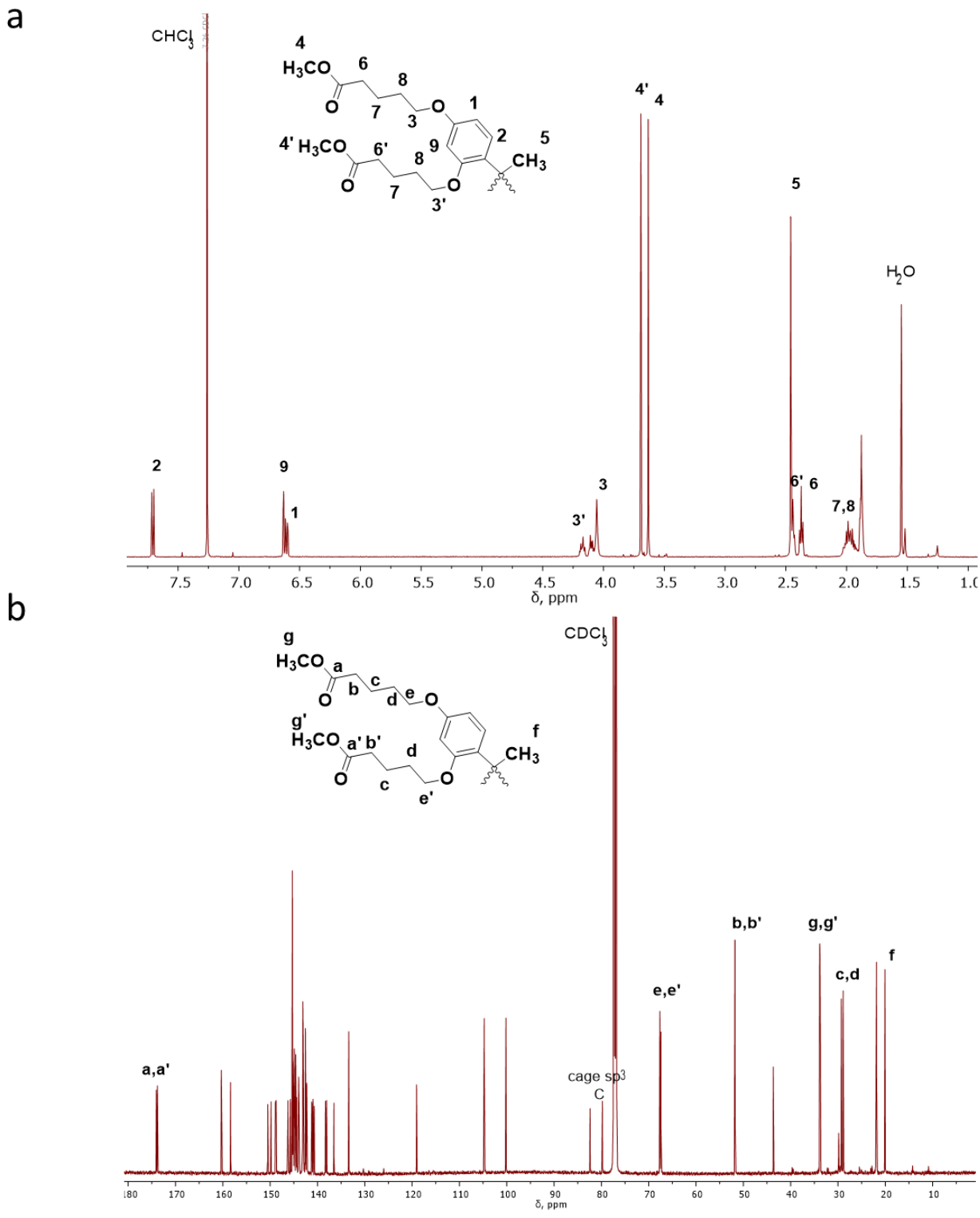

Figure S11. ^{1}H (a) and ^{13}C (b) NMR spectra of the fullerene derivative **F5**. Assignment of some signals is shown on the insets.

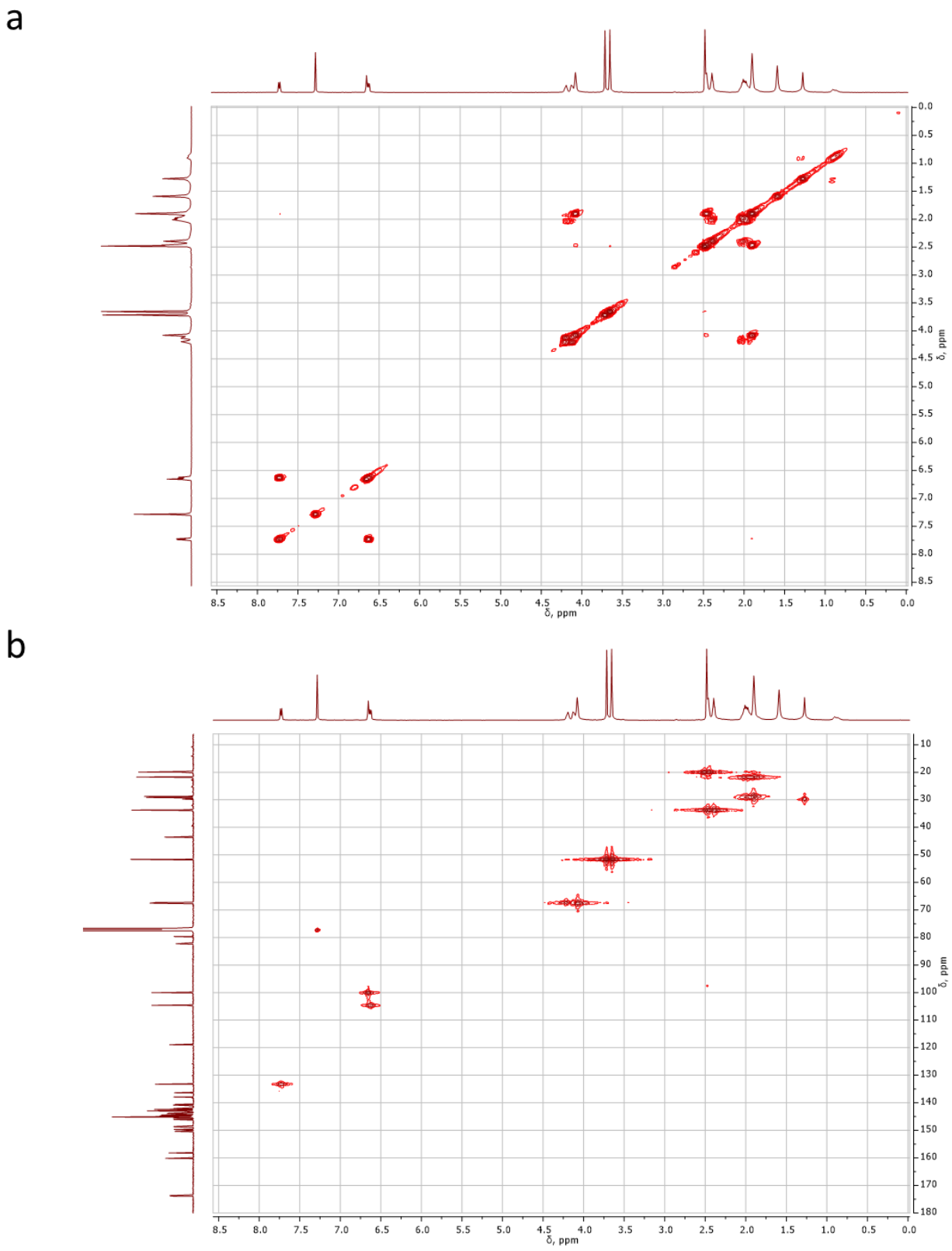

Figure S12. ^{1}H-^{1}H COSY (a) and ^{1}H-^{13}C HMQC (b) NMR spectra of the fullerene derivative **F5** ($CDCl_3$).

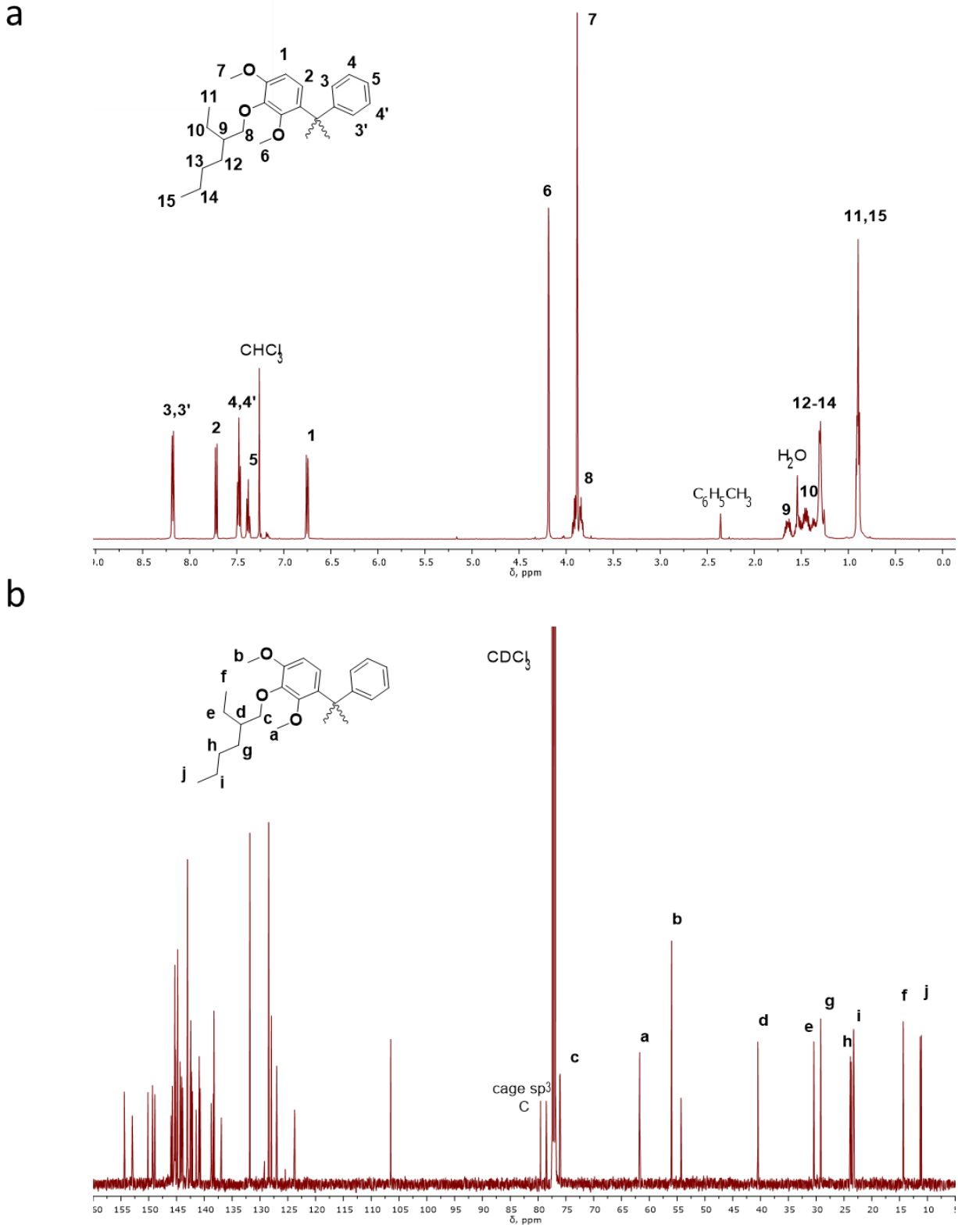

Figure S13. ^{1}H (a) and ^{13}C (b) NMR spectra of the fullerene derivative **F6**. Assignment of some signals is shown on the insets.

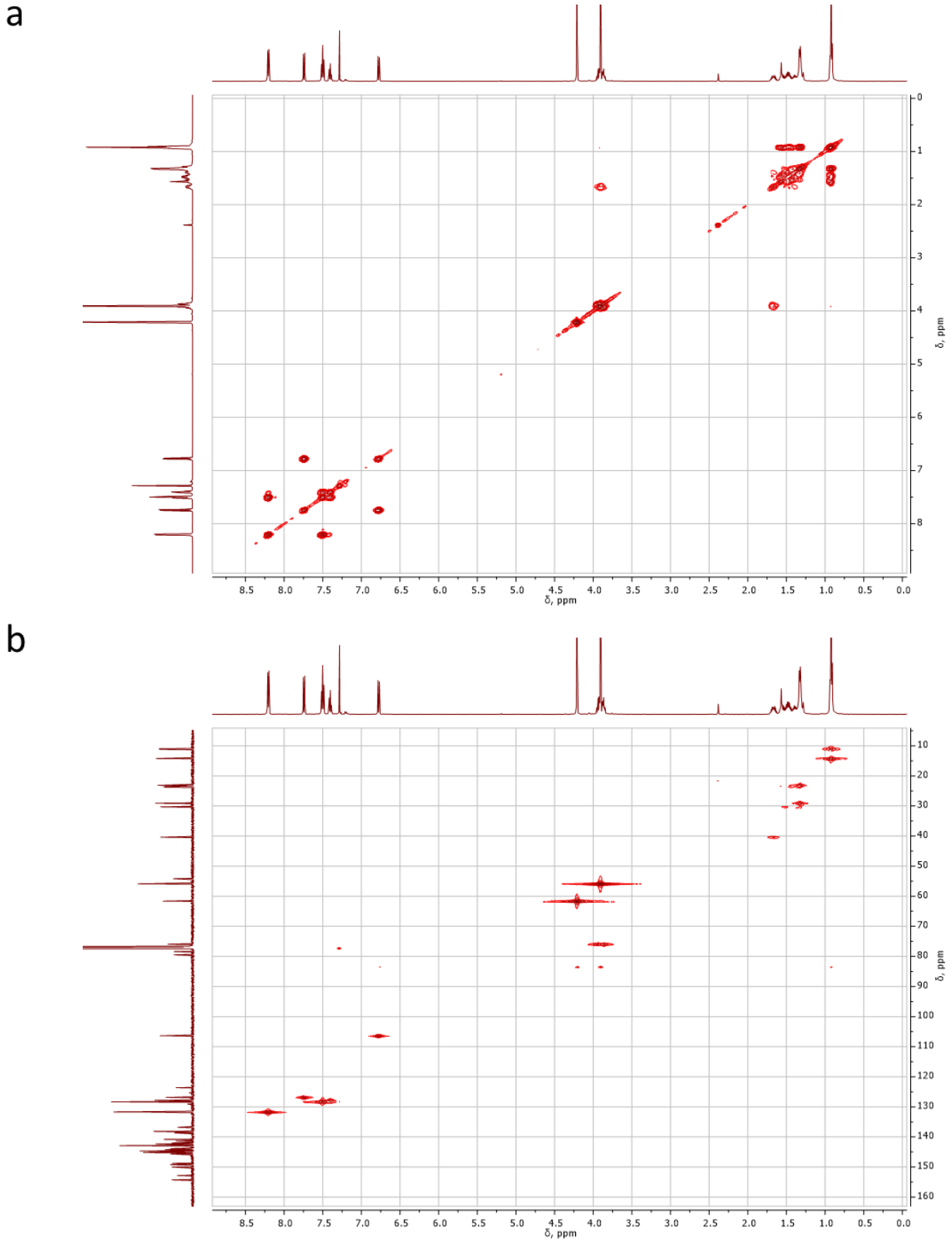

Figure S14. ^{1}H-^{1}H COSY (a) and ^{1}H-^{13}C HMQC (b) NMR spectra of the fullerene derivative **F6** ($CDCl_3$).

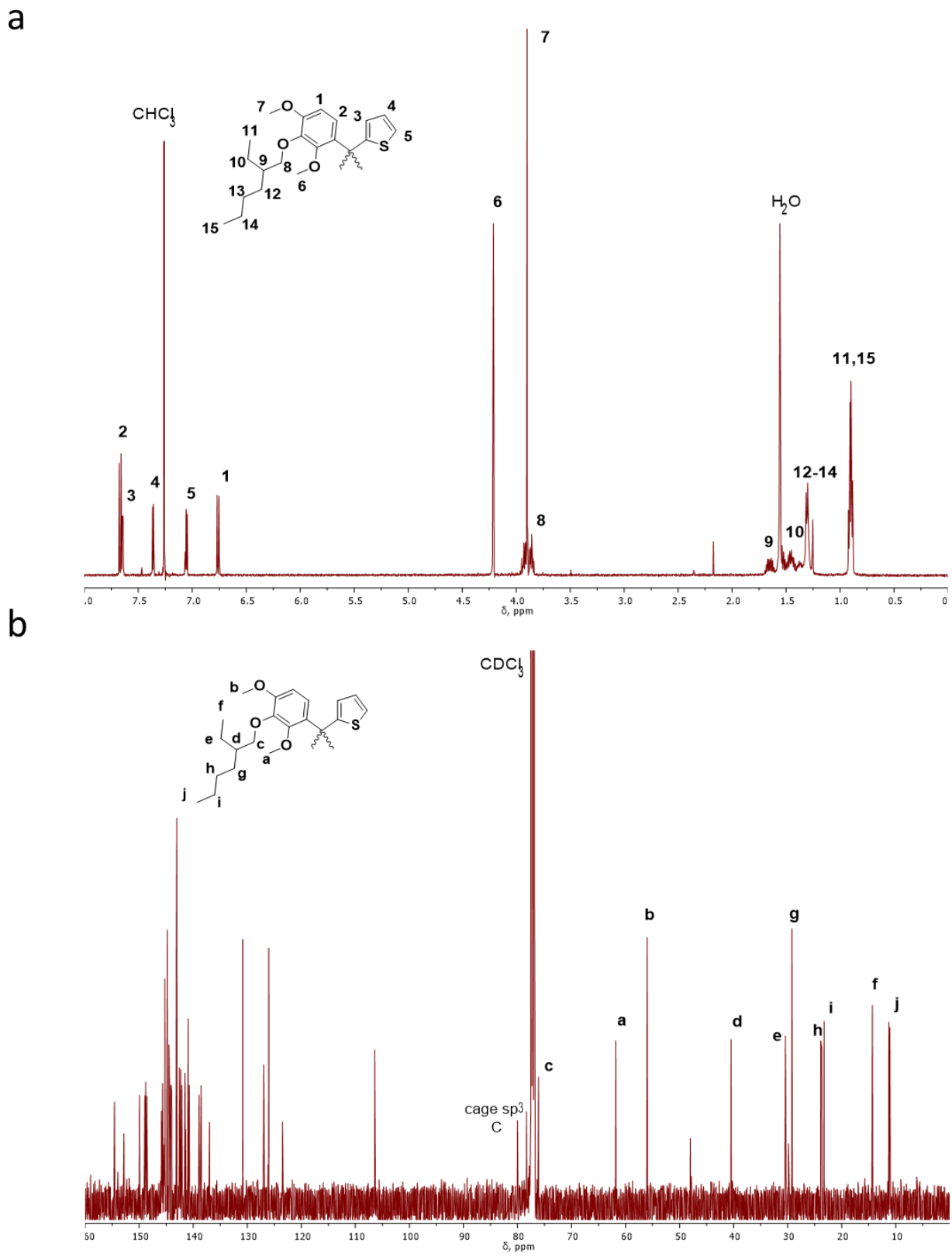

Figure S15. ^{1}H (a) and ^{13}C (b) NMR spectra of the fullerene derivative **F7**. Assignment of some signals is shown on the insets.

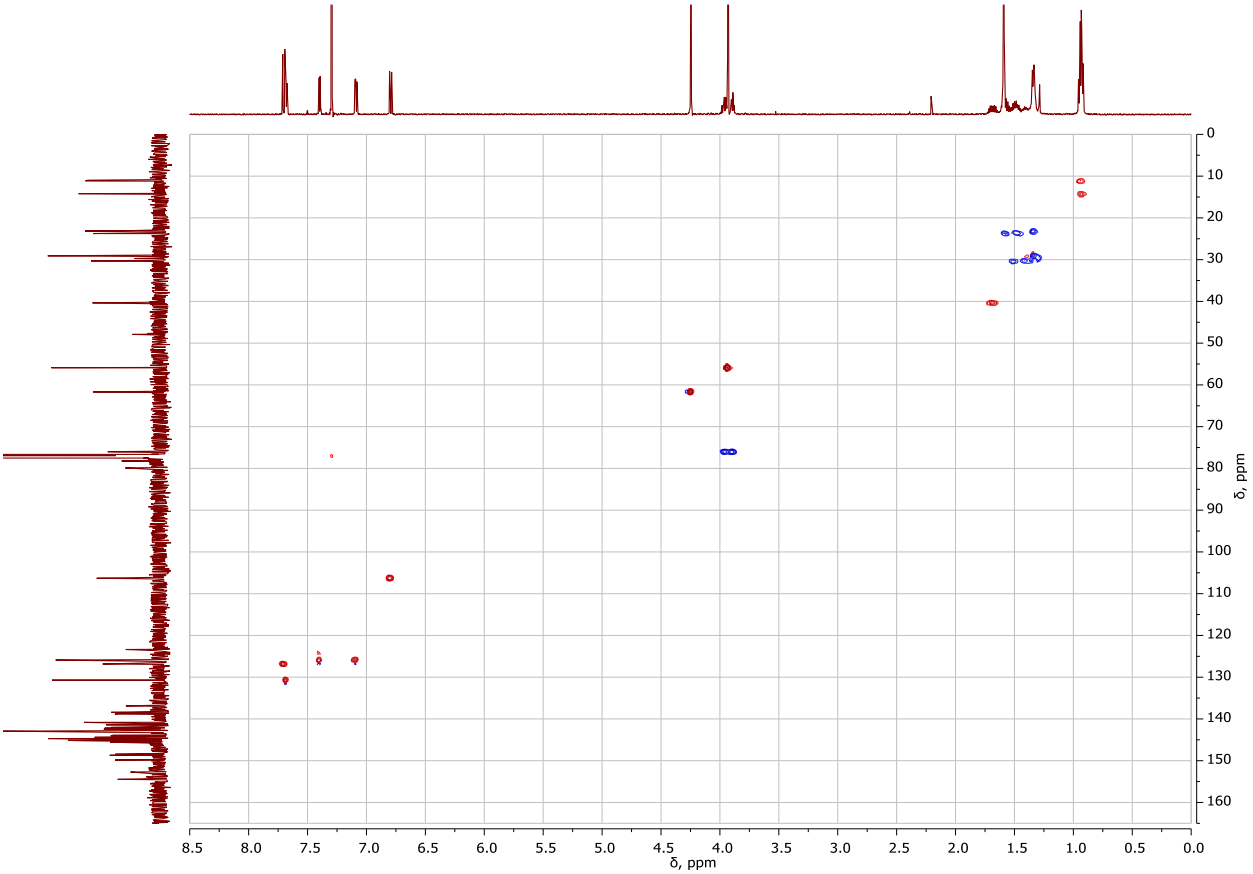

Figure S16. ^{1}H-^{13}C HSQC NMR spectrum of the fullerene derivative **F7** ($CDCl_3$).

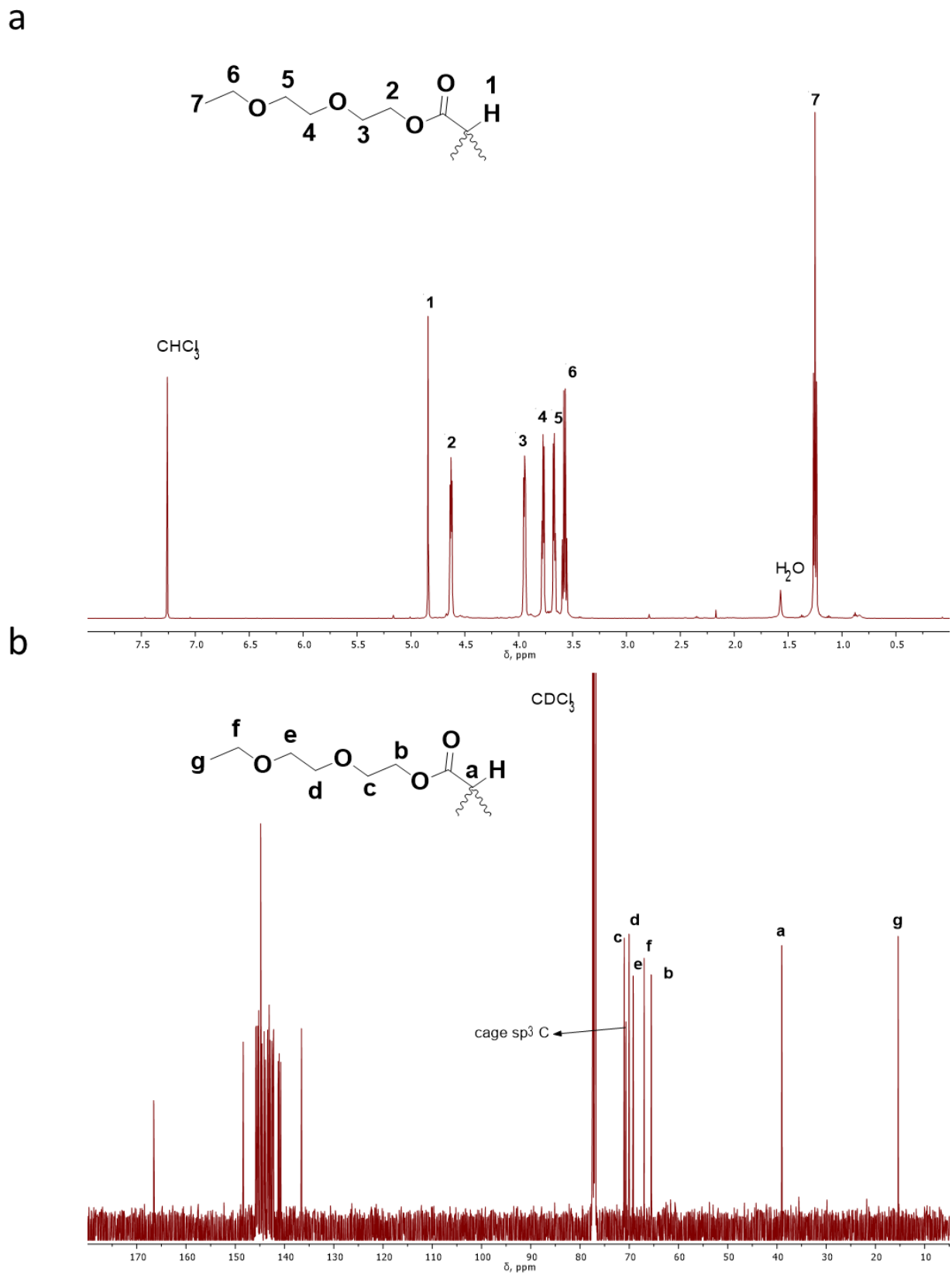

Figure S17. ^{1}H (a) and ^{13}C (b) NMR spectra of the fullerene derivative **F8**. Assignment of some signals is shown on the insets.

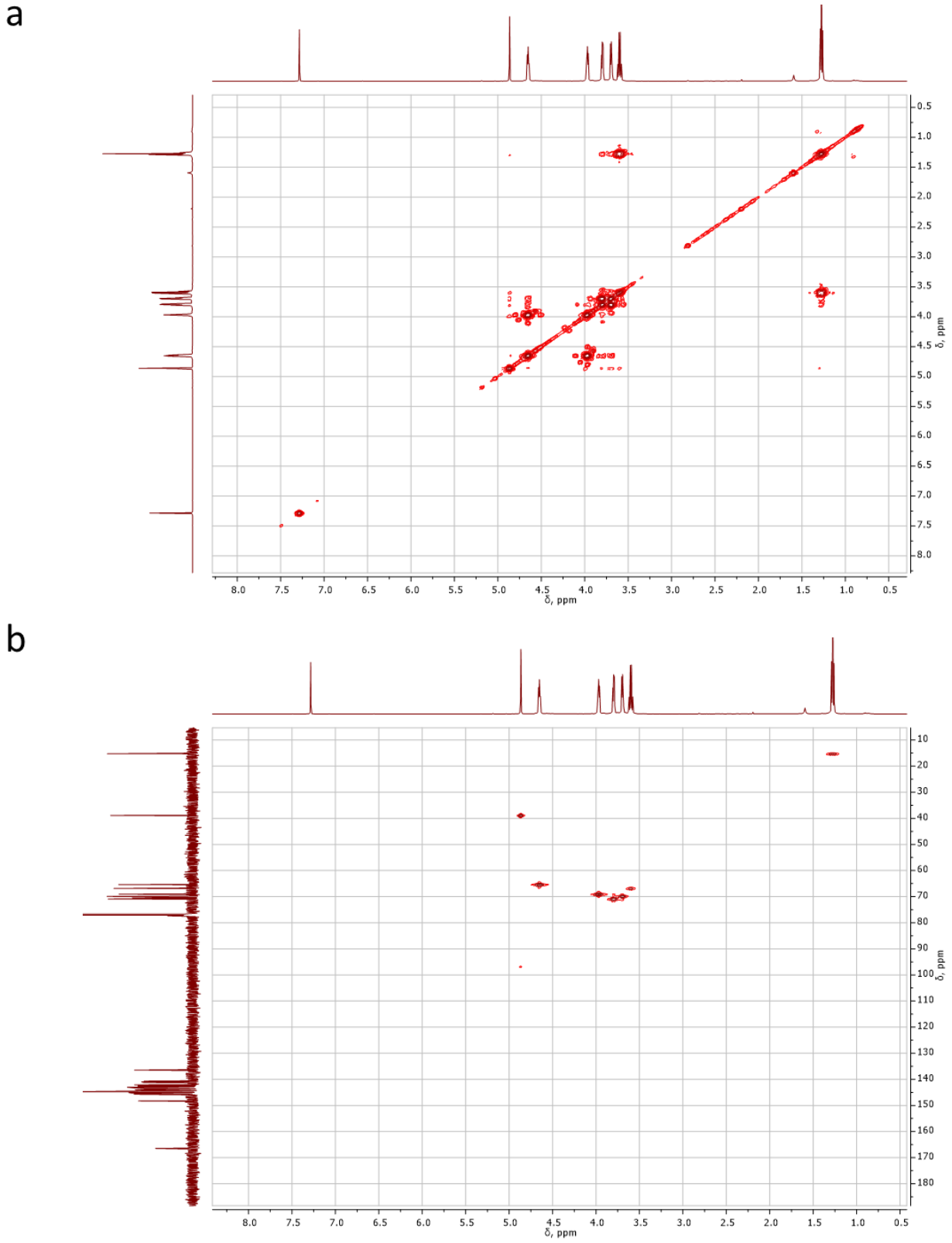

Figure S18. ^{1}H-^{13}C HSQC (b) NMR spectra of the fullerene derivative **F8** ($CDCl_3$).

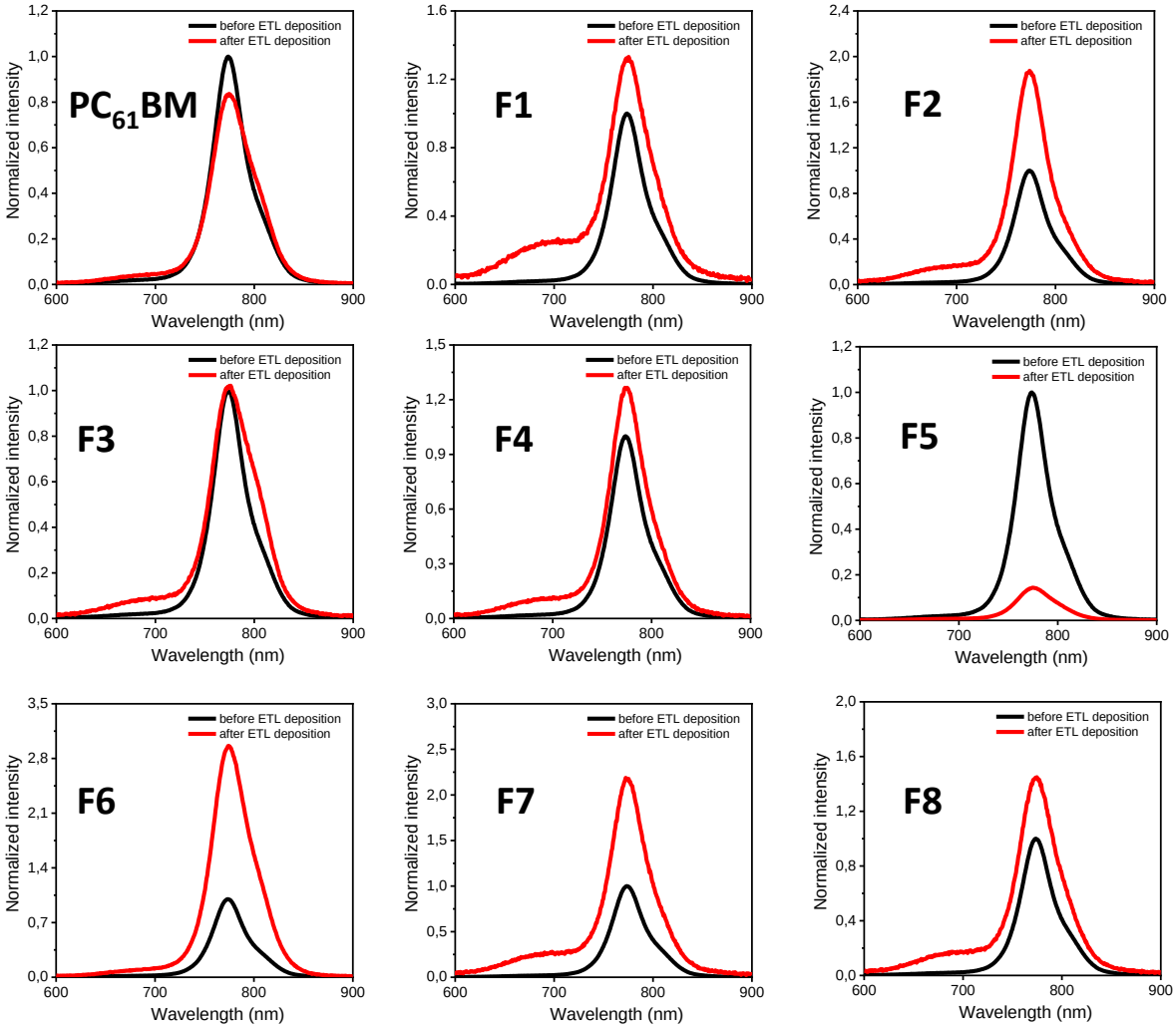

Figure S19. PL spectra of the lead halide perovskite films before (black line) and after (red line) deposition of fullerene-based ETLs.

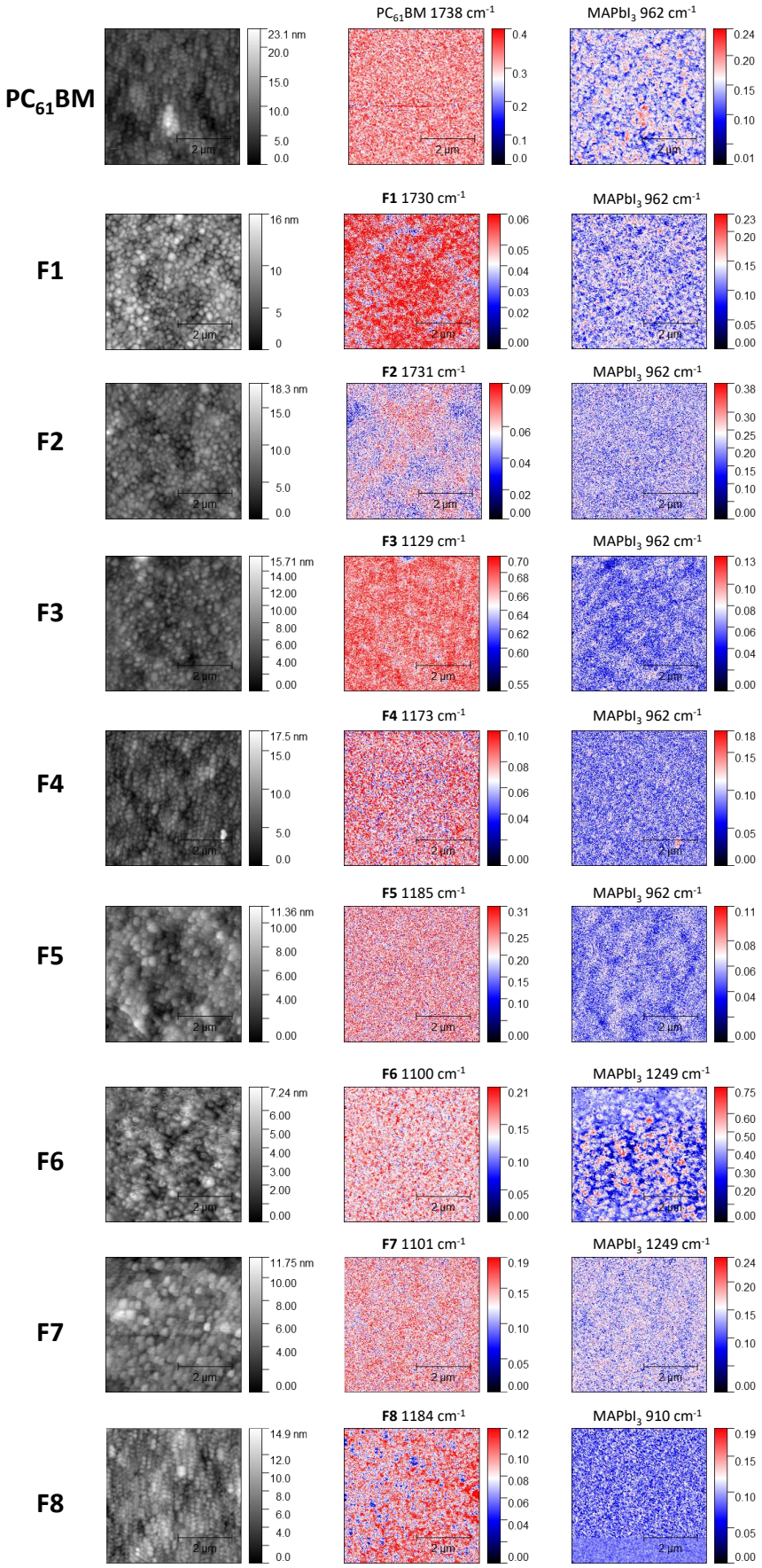

Figure S20. Overview of perovskite/ETL bilayer stack morphology: topography (left column) and IR s-SNOM images recorded at the characteristic frequencies of the ETL material (middle column) and perovskite absorber (right column). The used fullerene derivatives are listed on the left side.

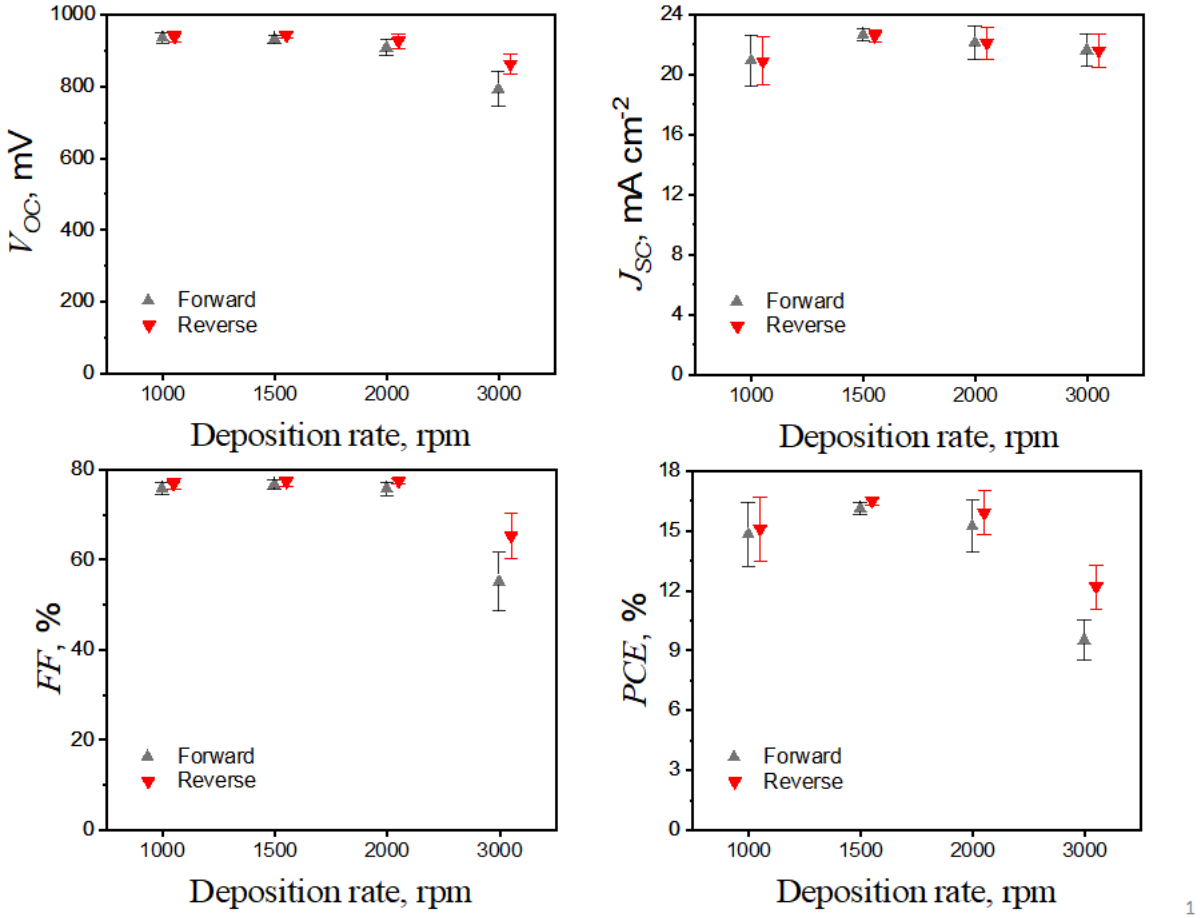

Figure S21. Dependence of the perovskite solar cell parameters on the deposition rate of the fullerene derivative **F1** (20.2 mg mL^{-1} solution in chlorobenzene) used to form electron transport layer in the devices